Self-sputtering of silver by mono- and polyatomic projectiles: A molecular dynamics investigation

M. Lindenblatt, R. Heinrich, and A. Wucher[a)]
Institute of Experimental Physics, University of Essen, 45117 Essen, Germany

B. J. Garrison
Department of Chemistry, The Pennsylvania State University, University Park, Pennsylvania 16802-6300

(Received 13 June 2001; accepted 30 July 2001)

The self-sputtering of silver under bombardment with Ag_m $(m=1,2,3)$ projectiles has been investigated by molecular dynamics (MD) simulation using the many body MD/MC-Corrected Effective Medium Potential developed by DePristo and co-workers. More specifically, the total sputtering yield as well as the mass distribution, i.e., the distribution of monomers and clusters within the flux of sputtered particles were calculated. For di- and triatomic projectiles, we observe a pronounced dependence of the calculated yields on the orientation of the incoming cluster, whereas the internuclear distance (and thus vibrational excitation of the projectile) does not seem to play a significant role. When averaged over the impact orientation, the calculated yields per projectile atom exhibit a distinct nonlinear enhancement when compared to the respective values calculated for monatomic projectiles of the same impact velocity. The abundances of nascent and final Ag_n clusters (identified immediately above and far away from the surface, respectively) within the sputtered flux are found to be significantly enhanced under polyatomic projectile bombardment, the effect increasing with increasing size of the sputtered cluster. Moreover, clusters produced under polyatomic bombardment appear to be colder, a finding which might be of considerable interest in the light of mass spectrometric surface analysis techniques. © *2001 American Institute of Physics.* [DOI: 10.1063/1.1404982]

I. INTRODUCTION

If a solid is bombarded with keV-ions, particles are released from the surface due to mostly elastic collisions, a process which is usually called sputtering. An interesting question in this context relates to the effects which might occur if the collision cascades initiated by several projectiles overlap in time and space. Due to the extremely short lifetime (~1 ps) and spatial extension (several nm, see below) of a collision cascade, such conditions can in practice only be realized if polyatomic species, i.e., clusters composed of several atoms, are used as projectile species. In a series of pioneering experiments, Andersen and Bay[1–3] as well as Thompson and Johar[4,5] have demonstrated that the total sputtering yield, i.e., the average number of atoms sputtered per impinging projectile, that is induced by a polyatomic projectile may significantly exceed the sum of the yields induced by the constituent atoms arriving separately with the same impact velocity. In a fairly recent review of this work, this observed nonlinearity of the sputtering yield was attributed to the occurrence of *collisional spikes*—characterized by a high density of moving atoms and therefore often also termed *thermal spikes*—as opposed to a plain superposition of *linear collision cascades* which are characterized by a low density of moving atoms (i.e., where every collision involves one moving atom and one atom at rest).[3] More recently, these experiments have been extended towards larger nuclearity (i.e., number of constituent atoms) and bombarding energy of the projectile clusters, where extremely high nonlinear yield enhancements of up to a factor of several 1000 in magnitude have been found.[6] In addition to yield measurements, a number of mass spectrometric experiments have revealed a significant influence of the projectile nuclearity on the composition of the flux of sputtered particles. These experiments, which to date have exclusively been performed on secondary ions, i.e., those particles which leave the surface in a charged state, have provided some indication that the contribution of clusters to the total flux of sputtered particles leaving the surface as a consequence of a projectile impact may be greatly enhanced if polyatomic instead of monoatomic projectiles are used, the effect being the more pronounced the larger the sputtered cluster.[7–11] These findings are of particular interest since the fundamental processes leading to the formation of cluster ejectees during a sputtering event are not yet fully understood.

The experimental findings of nonlinear effects induced by polyatomic projectiles are complemented by molecular dynamics computer (MD) simulations that have been performed for various surfaces bombarded with clusters of different compositions and sizes.[12–35] The size of projectile clusters employed in these studies ranges from diatomic species up to clusters containing thousands of atoms. In some cases, relatively large nonlinearities have been found,[16] whereas other work discerned only slight or no nonlinear yield enhancement when switching, for instance, from

[a)]Author to whom correspondence should be addressed. Fax: +49-201-183-93-4141; electronic mail: wucher@uni-essen.de

atomic to dimer projectiles.[25,35] Since most of the published work has been performed for a fixed size of the impinging clusters, a systematic investigation of the role the projectile nuclearity might play with respect to nonlinear enhancement effects is still lacking. This state of affairs is particularly true for the abundance pattern of sputtered clusters which are released following a polyatomic projectile impact. In this context, it is of great interest to determine (i) if a nonlinear enhancement of sputtering yield is generally accompanied by an increase of the cluster abundance and (ii) in how far the fairly unique correlation between the sputtered cluster abundance pattern and the sputtering yield that has been found for atomic projectiles[36–42] can be extrapolated towards polyatomic bombardment as well. In the present work, we aim at such a systematic study by employing MD simulations to model the impact of clusters with varying nuclearity onto a solid surface. In order to avoid any chemical complexity disturbing the collisional sputtering process and to keep the number of interaction potentials involved in the calculation as small as possible, we investigate the self-sputtering phenomena occurring at a single crystalline silver surface under bombardment with Ag_m projectiles. Silver was chosen as a target material mainly for two reasons. First, we have used the corresponding many-body interaction potential function in a number of previous simulations employing rare gas projectiles and found good correspondence with existing experimental data. Second, we wish to compare the results from the simulation with corresponding experiments on the self sputtering of a silver surface using Ag_m^+ primary ions which are currently under way in our laboratory.

II. DESCRIPTION OF THE CALCULATION

The molecular dynamics simulation employed to follow the elastic collision cascade initiated by the impinging projectile has been described in great detail earlier.[41,43,44] In short, the classical equations of motion are solved numerically for all atoms of a model fcc crystallite which in the present case has dimensions of $70\times70\times35$ Å and contains 10 500 metal atoms distributed over 15 atomic layers. The surface was assumed to be bulk terminated in the (111) direction with no reconstruction or relaxation, and open boundary conditions were employed on all faces of the crystal. The interaction among all atoms in the system was described by the MD/MC-CEM many-body potential originally designed by DePristo and co-workers.[45,46] In the context of the present investigation, the great advantage of this potential is twofold. First, it has been demonstrated that the MD/MC-CEM provides a realistic description of the binding forces between the atoms both within a small gas phase cluster and within a solid. Second, due to the fact that the repulsive (binary) part of the potential is derived from an *ab initio* dimer treatment, the potential can be directly employed for sputtering calculations without any modification to include a sufficiently repulsive interaction at small internuclear separations. In the present study, we use a specific potential fit to the properties of the silver dimer and solid silver.

The identification and classification of clusters among the flux of sputtered particles was done as described in detail in Refs. 41 and 47. Briefly, the trajectory integration of the collision cascade initiated by the impinging primary particle was terminated at a time when either the total energy of all atoms within the model crystal had fallen below zero or a preset integration time limit (mostly 3 ps) was reached. Upon termination, the list of ejected atoms obtained for a given primary ion impact was examined for ''nascent'' clusters, i.e., agglomerates of two or more atoms with negative total energy,

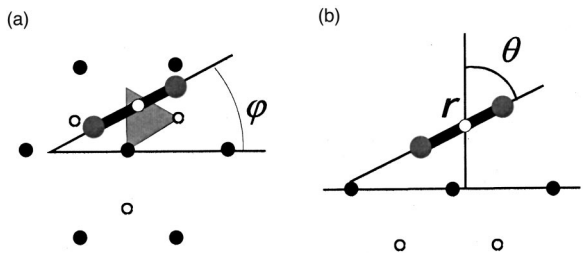

FIG. 1. Schematical view of dimer impact orientation parameters: (a) (111) surface view; (b) side view. Closed symbols correspond to first layer atoms, open symbols depict second layer atoms.

$$E_{\text{tot}}^{\text{cluster}}=\sum_{i=1}^{n} E_i^{\text{rel}}+V_i\,, \tag{1}$$

which were then subjected to a stability check against dissociation as described in detail in Refs. 41 and 47. Unstable clusters with internal energies,

$$E_{\text{int}}=E_{\text{tot}}^{\text{cluster}}+E_a \tag{2}$$

above the dissociation threshold E_d (i.e., the lowest threshold for unimolecular fragmentation as determined from the difference of atomization energies E_a of parent and fragment clusters; for values of E_a and E_d, see Ref. 41) were investigated by further MD simulation until only stable fragments remained. These ''final'' clusters are of particular interest since they represent those sputtered species that are sampled by experimental schemes detecting the particles at times of typically several microseconds after their ejection from the surface.

The simulations were performed for Ag_m projectiles with $m=1$, 2, 3 normally incident onto a silver (111) surface. As outlined in the introduction, nonlinear effects are identified by comparing the results obtained for projectiles of different size that impinge onto the surface with the same impact velocity (or kinetic energy per constituent atom).[3] In order to allow comparisons under such conditions, different total kinetic energies of 2, 4, and 6 keV were employed for monatomic, diatomic, and triatomic projectiles, respectively. Most of the calculations were done with a set of 120 trajectories with impact points (i.e., surface points towards which the center-of-mass velocity of the projectile was directed) being uniformly distributed over the smallest irreducible surface cell. Polyatomic cluster impacts were characterized by additional parameters describing the structure and orientation of the projectile. For the case of diatomic species, these are the internuclear separation r, polar angle θ and azimuth φ as indicated in Fig. 1. In order to examine the role of these parameters, a number of different trajectory sets

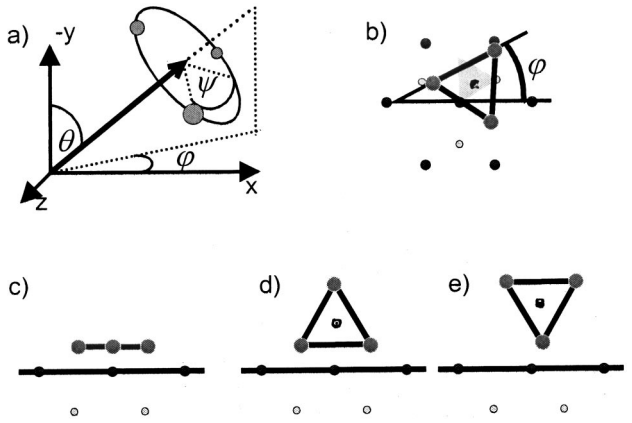

FIG. 2. Schematical view of impact orientation parameters relevant for a triatomic projectile: (a) definition of Euler angles; (b) azimuth angle; (c) planar incidence; (d) and (e) perpendicular incidence. Closed symbols correspond to first layer atoms, open symbols depict second layer atoms.

were calculated (for one specific total kinetic impact energy of 4 keV), where one parameter was varied while the others were kept constant. Triatomic projectiles were assumed to exhibit the equilibrium structure determined by the MD/MC-CEM interaction potential (an equilateral triangle with a side length of 2.64 Å). For these species, the impact orientation was characterized by three Euler angles θ, φ, and ψ which are defined in Fig. 2(a). For the specific case of $\theta=90°$ (i.e., where the threefold symmetry axis of the equilateral triangle is oriented parallel to the surface), two different impact orientations corresponding to the internal rotation angles $\psi=0°$ and $\psi=180°$ were tested with the azimuth φ fixed at an arbitrary value of $\varphi=0°$. In these cases, which will in the following be referred to as ''perpendicular incidence,'' the equilateral triangle hits the solid either with its base or with its tip pointing towards the surface [cf. Figs. 2(d) and 2(e)]. In a second set of simulations, the polar angle was kept fixed at $\theta=0°$. In these cases, which will in the following be referred to as ''planar incidence,'' the trimer is oriented parallel to the surface, and the azimuth angles φ and ψ coincide. Due to the threefold symmetry of the projectile, the azimuth range between 0° and 120° is sufficient in order to cover the whole orientational space for this polar angle orientation. This range was sampled by arbitrarily selecting a total of six different values of φ.

In order to facilitate enough statistics to reveal the rapidly falling size distribution of final clusters, a large set of 3200 trajectories were run for the specific cases of a monomer impinging with an energy of 2 keV. For the dimer and trimer projectiles, all simulations performed at impact energies of 4 keV (dimers) and 6 keV (trimers) were combined for the determination of the cluster size distribution. In an attempt to ensure that the limited integration time or the limited size of the model crystal do not influence the results, selected trajectories which resulted in very high atomic and cluster emission yields were rerun with a larger crystal (containing up to 24 000 atoms) and integrated for longer times (up to 7 ps).

III. RESULTS AND DISCUSSION

In order to discern nonlinear enhancement effects induced by the polyatomic character of the projectiles, we will compare the results obtained for different projectiles impinging onto the surface with the same impact velocity. Under these conditions, a plain superposition of linear collision cascades initiated by the different constituent atoms of the projectile would result in observables which simply represent the sum of the respective quantities determined for the constituents impinging independently. Every deviation from this sum therefore constitutes a nonlinear effect, and the ratio between an actually determined observable and the hypothetical sum value will hence be called an ''enhancement factor.'' Note that this factor does not necessarily have to be larger than unity.

The discussion will focus on five observables which are extracted from the list of sputtered particles output from the MD simulation. For each of these, we will proceed in the order of complexity, starting with monatomic and working our way towards triatomic projectiles. The most readily accessible observable is of course the average sputtering yield. Moreover, it is mainly this quantity which has been frequently demonstrated experimentally to exhibit nonlinear enhancements. In the first subsection, we therefore present the average sputtering yield obtained under atomic, diatomic, and triatomic projectile bombardment. As outlined in the Introduction, the second observable which has been suggested to exhibit nonlinear effects is related to the occurrence of clusters within the flux of particles sputtered from the surface. While the nascent clusters (identified immediately above the surface) reveal most direct information about the collisional sputtering process itself, they are mostly unstable on a very short time scale and therefore inaccessible to experimental detection. Final clusters (identified far away from the surface), on the other hand, represent the stable products of unimolecular fragmentation chains undergone by unstable nascent species and are therefore tractable by experimental detection schemes. In order to determine whether cluster abundances are nonlinearly enhanced, we will in the second subsection therefore evaluate the size distribution of both nascent and final clusters ejected from the surface following projectile impacts of different nuclearity. As a third quantity that is in principle accessible by experiment, we then determine the kinetic energy distribution of sputtered monomers (atoms). This distribution is of much interest since it has been suggested that the occurrence of spike effects should lead to a systematic deviation from the energy distribution predicted by linear cascade theory. The last two subsections will then be devoted to the internal energy distribution of sputtered clusters and the radial distribution of the ejection probability of surface atoms around the projectile impact point. Both observables are inaccessible by experiment, but may reveal valuable information about the nature of the collisional processes leading to the sputter ejection of particles initiated by impact of different projectiles.

A. Average sputtering yields

In order to evaluate the average sputtering yield, all sputtered atoms identified in a particular simulation were counted

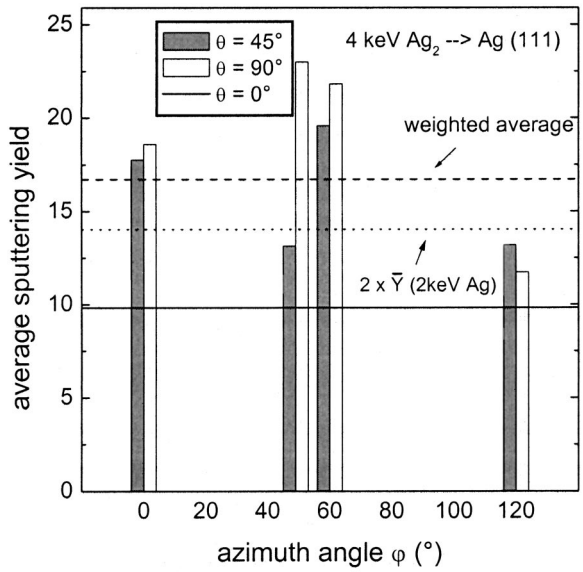

FIG. 3. Average sputtering yield calculated for diatomic projectiles of 4 keV impinging under various different orientation angles. Solid line: perpendicular incidence (where azimuth is meaningless); dashed line: weighted average calculated according to Eq. (3); dotted line: doubled average yield of monatomic projectiles impinging with the same velocity.

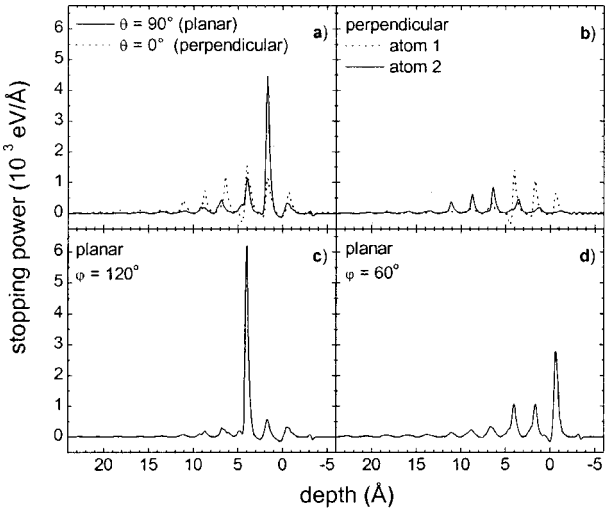

FIG. 4. Energy loss of projectile atoms vs depth below the surface for a diatomic projectile impinging with different orientation: (a) planar (φ=0°) and perpendicular incidence (summed over both constituent projectile atoms); (b) separate plots for constituent projectile atoms 1 and 2 for perpendicular incidence; (c) planar incidence (φ=60°) (summed over both constituent projectile atoms); (d) planar incidence (φ=120°) (summed over both constituent projectile atoms). The zero of the depth scale is located at the position of the uppermost atomic layer.

(regardless of their bond state) and divided by the number of trajectories run in this simulation. Due to the fact that projectile and target atoms are the same, the resulting yield value was corrected by the number of atoms contained in the projectile. The resulting total sputtering yield that was obtained for monatomic projectile impact at 2 keV amounts to $\bar{Y}=7.0$ atoms/projectile. This value is in very good agreement with existing literature data on the experimental value of the self-sputtering yield of (polycrystalline) silver under bombardment with Ag^+ ions that have been measured by Almén and Bruce,[48] a finding which strongly supports the validity of the employed interaction potential.

Figure 3 depicts the total sputtering yields calculated for bombardment with Ag_2 projectiles as a function of the impact orientation. More specifically, the yield data has been plotted as a function of the azimuth angle φ for different values of the polar angle θ. For the specific case of perpendicular incidence (θ=0°), a solid line has been introduced since for this case the impact azimuth is meaningless. It is clearly seen that the impact orientation significantly influences the sputtering action. If the collision cascades induced by the two constituent atoms of the projectile would linearly superimpose, the yield expected under these conditions should correspond to twice the yield calculated for atoms impinging with the same impact velocity, i.e., with half the impact energy. In order to discern nonlinear yield enhancements, the respective linear value (twice the atom bombardment yield calculated for an impact energy of 2 keV) has been included in the figure (dotted line). It is seen that the largest nonlinear enhancement is found for projectiles orientated parallel to the surface with an azimuth of approximately 50°. In contrast, dimers impinging perpendicular to the surface lead to a sublinear *decrease* of the sputtering yield. A calculation of a second set of trajectories with slightly displaced impact points reveals that these variations are not caused by insufficient statistics of the simulation, but rather reflect real changes in the sputtering action. In order to examine the reason for this behavior, Fig. 4 shows the vertical stopping power, i.e., the energy lost by the projectile atoms as a function of depth below the surface, averaged over all trajectories of the respective simulation. Apart from some artificial structure induced by the cutoff of the interaction potential at some distance above the surface, the equidistant peaks visible in the curves correspond to the energy loss at the discrete atomic layers within the solid. Comparison of the two curves displayed in Fig. 4(a) reveals that a vertically impinging dimer deposits its energy deeper within the bulk, thus leading to less energy density at the surface than under planar impact conditions. The reason for this behavior is illustrated in Fig. 4(b), which shows the energy loss of both constituent atoms of the projectile separately.

It is seen that the first atom deposits its energy predominantly in the uppermost three atomic layers, thereby apparently pushing surface atoms aside and ''clearing the way'' for the following second atom. Similar effects have also been observed by Yamamura *et al.*[12] As a consequence, the second atom penetrates the first few atomic layers and deposits its energy deeper within the bulk, thus leading to a larger average depth of energy deposition and, hence, less sputtering action at the surface. The azimuth variations for planar incidence can also be qualitatively understood in terms of stopping power arguments. For φ=0°, both atoms of the dimer projectile impinge into surface areas where no atom of the first monolayer but atoms of the underlying second monolayer can be closely hit. Therefore, most of the projectile energy is lost in the second atomic layer [see Fig. 4(a)]. At φ=120°, only atoms located in the third atomic layer can be directly hit by the projectile atoms, and the projectile energy

is therefore deposited deeper within the solid, thus leading to less sputtering action [see Fig. 4(c)]. In contrast, at $\varphi=60°$ both projectile atoms may directly hit surface atoms, thus leading to a preferred energy loss within the uppermost atomic layer [Fig. 4(d)].

If the calculated yield values are to be compared to experiments, the data displayed in Fig. 3 must be properly averaged. In principle, the averaging procedure should weigh the different yield values according to the statistical probability of a projectile cluster approaching the surface with a particular orientation which, in turn, will depend on the way the projectile clusters are generated. Assuming a randomly orientated cluster beam, we arrive at the following expression describing the averaged sputtering yield for a diatomic projectile impact as

$$\langle Y\rangle = \frac{1}{\Sigma_i Z_i \sin\theta_i}\left(\sum_i \sum_j \overline{Y}_{\mathrm{MD}}(\theta_i,\varphi_j)\sin\theta_i\right), \qquad (3)$$

where Z_i denotes the total number of azimuth values φ_j calculated for a particular polar angle θ_i. The resulting average sputtering yield is depicted in Fig. 3 as a dashed line. It is seen that this value is quite significantly above the dotted line corresponding to a linear superposition of two independent collision cascades initiated by two independent atomic projectiles of 2 keV. The simulations therefore clearly indicate a measurable nonlinear yield enhancement of about 19% for a diatomic projectile impact.

An interesting parameter to investigate is the internuclear distance r between the atoms in an impinging cluster. This quantity is particularly important in view of the fact that any polyatomic projectile cluster generated in an experiment will inevitably contain a certain amount of vibrational excitation, thus leading to a statistical distribution of internuclear distances around the gas phase equilibrium value. In order to elucidate the role of this parameter, Fig. 5(a) shows the variation of the total sputtering yield calculated for a diatomic projectile impinging under $\theta=\varphi=0°$ as a function of the distance between the two projectile atoms. It is apparent that, apart from variations that fall within the statistical relevance of the data, the internuclear distance has practically no influence on the resulting sputtering action. In order to illustrate the implication of this finding with respect to vibrational excitation, Fig. 5(b) shows the gas phase Ag_2 dimer interaction potential as given by the MD/MC-CEM parametrization employed here. It is apparent that the explored range of internuclear distances covers the complete interval that is accessible by vibrational excitation of the impinging dimer. Since the absolute magnitude of the vibrational energy is always negligible compared to the kinetic energy introduced by the projectile, we therefore conclude that vibrational excitation of polyatomic projectiles has no effect on the sputtering phenomena induced by such particles.

The total sputtering yield calculated for trimer projectiles impinging with an energy of 6 keV is exemplified for three selected impact orientations in Fig. 6(a). For comparison, the tripled yield determined for monatomic as well as 3/2 times the yield determined for diatomic projectiles of the same impact velocity have been included as dotted lines. In order to investigate the role of the azimuthal orientation, Fig.

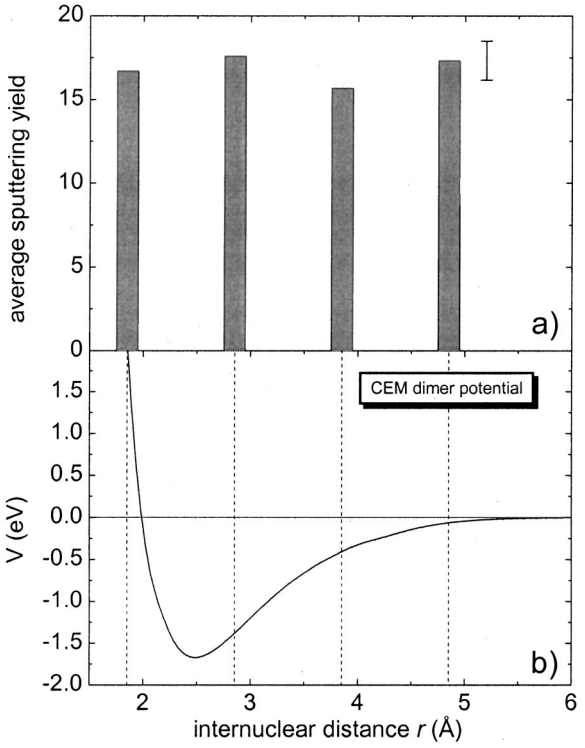

FIG. 5. Average sputtering yield induced by diatomic projectiles impinging under $\theta=\varphi=0°$ vs internuclear distance between the two projectile atoms (a) and internuclear interaction potential of a gas phase diatomic projectile as given by the MD/MC-CEM parametrization (b).

6(b) depicts the calculated yield as a function of $\varphi=\psi$ for planar incidence. It is seen that the relative variation is less pronounced than that observed in Fig. 3, thus indicating that the influence of impact orientation may decrease with increasing projectile cluster size. In view of the increased symmetry of larger projectiles, this finding may appear reasonable, although much more data are needed in order to clarify this point. From the data presented in Fig. 6, it is evident that all investigated impact orientations correspond to a nonlinear increase of the sputtering yield with respect to monatomic and diatomic projectiles. If the yield is to be averaged over the impact orientation, the statistical probabilities of finding different projectile orientations must in principle again be used as weight parameters. We are, however, not aware of any straightforward way to determine these probabilities [such as given by Eq. (2) for the diatomic case] and therefore chose to calculate the average sputtering yield (as well as all other averaged observables extracted from the simulations) by simply giving each simulated orientation the same weight. The resulting average yield for trimer projectiles is included in Fig. 6 as a dashed line. Comparing this value to that expected from a linear superposition of three independent collision cascades initiated by atomic projectiles of 2 keV (dotted line in Fig. 6) reveals a pronounced nonlinear yield enhancement of 49%.

The yield enhancements deduced here can be compared to those obtained by Shapiro and Tombrello who studied the self-sputtering of gold with mono-, di-, and triatomic gold projectiles of 100 and 200 keV/atom using MD computer simulation.[18] In this work, nonlinear enhancements of 37%–

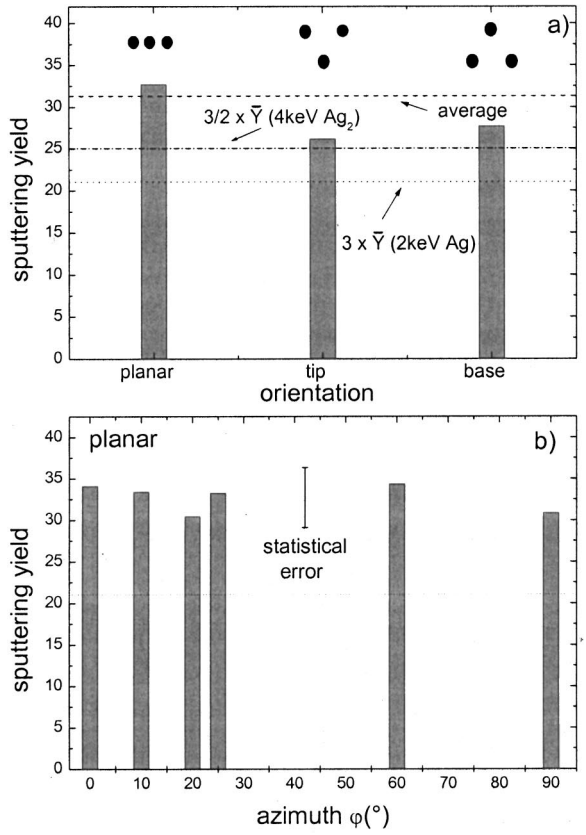

FIG. 6. Average sputtering yield induced by triatomic projectiles impinging under different orientation with respect to the surface: (a) planar, tip and base incidence (see Fig. 2 and text); (b) planar incidence with varied azimuth.

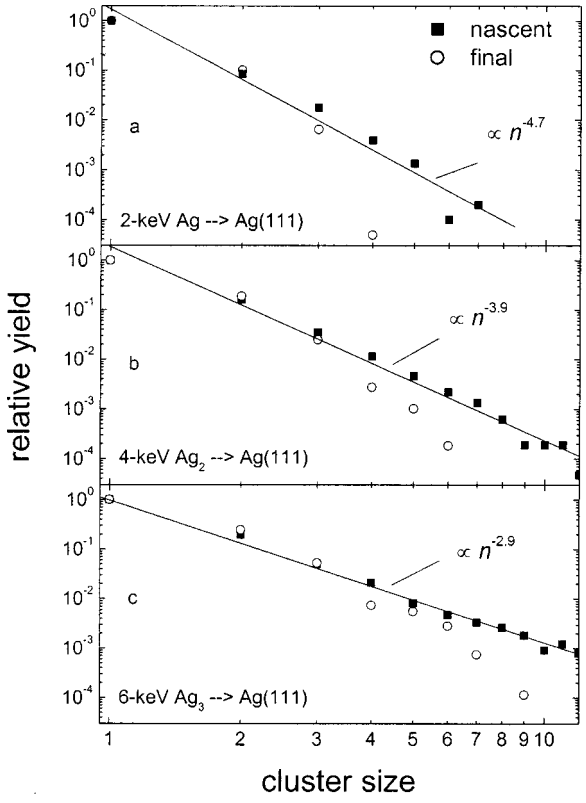

FIG. 7. Relative yields of nascent and final Ag_n clusters sputtered from a silver (111) surface under bombardment with (a) monatomic; (b) diatomic; (c) triatomic projectiles of the same velocity corresponding to a kinetic impact energy of 2 keV/atom.

44% and of 39%–92% were found for diatomic and triatomic projectiles, respectively. In view of the large difference in kinetic energy per atom, the relatively close agreement with the results presented here seems to be surprising. It should be noted, however, that the yield enhancements disclosed in Ref. 18 significantly underestimate the corresponding experimental data.[6]

B. Mass distribution

Due to the absence of atoms of any other chemical element except silver, the mass distribution of sputtered particles must exclusively be composed of Ag atoms and Ag_n clusters. Figure 7 shows the relative yields, i.e., the partial yields normalized to that of sputtered monomers, of secondary nascent and final Ag_n clusters which are produced under bombardment with monatomic, diatomic, and triatomic projectiles of 2 keV, 4 keV, and 6 keV, respectively, as a function of the cluster size. In order to arrive at enough statistics, the results of all simulations performed for polyatomic projectiles of these particular impact energies (i.e., the calculations for different impact orientations and internuclear distances) have been combined. It is seen that the distribution of nascent clusters can in all three cases be approximated by a power law size dependence according to

$$Y(n) = Y_n / Y_1 \propto n^{-\alpha}. \tag{4}$$

This finding is well in accordance with our previous simulations performed for bombardment with atomic rare gas projectiles[41] as well as with other MD simulations on the self-sputtering of gold with mono- and polyatomic projectiles of 100 keV/atom.[17] Due to the influence of fragmentation, the size distribution of final clusters falls steeper with increasing cluster size than that of the nascent clusters. Again, this behavior is in good agreement with our previous results. In principle, it is of interest to determine the connection between the cluster size distribution and other quantities characterizing the sputtering process. In all cases investigated so far, it has been observed both experimentally[36–40,49–51] and by MD simulation[41,47,52,53] that whenever the sputtering conditions were changed such as to result in a higher average yield, the abundance of sputtered clusters was increased, thus leading to a lower apparent value of the power law exponent. Due to the limited dynamic range determined by the statistics of the simulations performed here, final clusters could only be identified up to a size of $n=4$ for atomic, $n=6$ for diatomic, and $n=9$ for triatomic projectiles. Although it is in principle possible to fit a power law similar to Eq. (4) to these distributions, the exponent δ delivered from such a fit will depend on the available range of cluster sizes which, in turn, is different for different projectiles. In order to allow a more quantitative comparison, we therefore chose to plot the decay exponent α (characterizing the distribution of *nascent* clusters) against the average sputtering yield. The results are presented in Fig. 8 together with

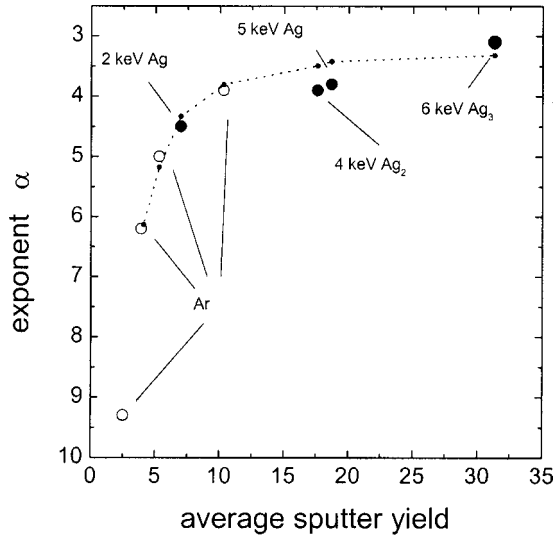

FIG. 8. Power law exponent α describing the size distribution of nascent clusters. The data have been plotted against the average sputtering yield in order to illustrate a general correlation between the cluster abundance pattern and the sputtering parameters (see text). Closed symbols: monatomic, diatomic, and triatomic silver projectiles of 2 keV/atom (this work); open symbols: Ar projectiles (data taken from Ref. 41); dotted line: dependence predicted from the statistical emission probabilities according to Eq. (7) in the text.

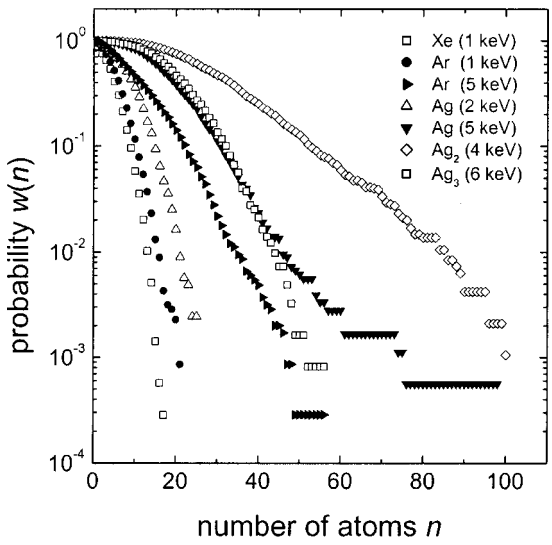

FIG. 9. Statistical probability distribution for emission of at least n atoms in a single projectile impact under bombardment of an Ag(111) surface with monatomic, diatomic, and triatomic silver projectiles of 2 keV/atom (this work), 1 keV Ar, 1 keV Xe, and 5 keV Ar projectiles (data taken from Ref. 41).

similar data taken from Ref. 41. It is seen that the exponents determined here fit nicely into the earlier data, thus emphasizing the apparent general correlation between the cluster abundance distribution and the sputtering yield. In order to illustrate the physical reason for this behavior, we revert to the statistical nature of the sputtering process. A particular projectile impact will induce an individual sputtering yield Y which is statistically distributed according to a probability distribution $P(Y)$ that can easily be deduced from the simulations. The average sputtering yield is connected to this distribution via

$$\overline{Y} = \sum_{Y=0}^{\infty} Y \cdot P(Y). \tag{5}$$

It is clear that the formation and emission of a sputtered cluster containing n atoms in a particular sputtering event ultimately requires the emission of at least n atoms in the course of this event. As a necessary (but not sufficient) condition for cluster emission we therefore evaluate the probability $w(n)$ that at least n atoms are ejected as a consequence of a particular projectile impact as[53]

$$w(n) = \sum_{Y=n}^{\infty} P(Y). \tag{6}$$

Figure 9 shows the resulting distributions for the different sputtering conditions employed here and in our previous simulations.[41] It is apparent that the probability to fulfill the number requirement is larger for larger average yields. As seen in Fig. 8, on the other hand, the effect tends to saturate in the limit of high yields. This finding is also supported by the high energy gold self sputtering simulations, where identical values of $\alpha \sim 2.3$ have been found for mono-, di-, and triatomic projectiles of 100 keV/atom, although the corresponding average sputtering yields increased greatly from 70 to 369, respectively.[17] One can try to illuminate this saturation by assuming a direct linear relation between $w(n)$ and the relative yield of nascent sputtered Ag_n clusters (which of course constitutes a large oversimplification since the correlated motion of n atoms which is necessary to form and survive the emission as a bound cluster is completely ignored). With this assumption, the power law exponent α is expected to scale with the probability w as

$$\alpha \approx -\frac{\ln[w(n)] - \ln[C]}{\ln[n]}, \tag{7}$$

where C denotes the proportionality constant in the above mentioned linear relation. For an arbitrarily selected value of $n=17$, a corresponding plot of Eq. (7) has been included as a dotted line in Fig. 8. In order to match with the actually determined exponents, the constant C was chosen as 10^{-4}, a variation of this value will however only shift the curve vertically but not alter the predicted yield dependence. It is seen that the dependence of α on the average sputtering yield is reproduced very well. For other values of n, the constant C must be slightly modified, but otherwise the general trend remains the same. Although the argument is at best semiquantitative, it is therefore apparent that particularly the observed saturation of the power law exponent towards high yields is completely understandable in terms of the statistical emission probability distribution.

Probably the most important observation in Fig. 7 is the fact that the relative abundance of clusters among the flux of sputtered particles is significantly enhanced when changing from monatomic to polyatomic projectiles. Moreover, it is seen that the magnitude of this enhancement increases with increasing size of the sputtered cluster, a trend which may be expected to continue towards larger clusters. The results from the simulations appear to be in qualitative agreement with a number of experimental investigations, where a sig-

nificant nonlinear enhancement of the relative abundance of sputtered cluster ions was found for polyatomic projectile bombardment.[8,11,54–64] In particular, we can compare the results obtained here with published experimental data on the relative abundance of clusters within the flux of secondary ions sputtered from polycrystalline Ta and Nb foils under bombardment with polyatomic gold projectiles. For the range of final cluster sizes accessible in this work, we find in most cases a fair agreement of the relative enhancement factors. Comparing, for instance our data obtained for 2 keV/atom with the transitions from 6 keV Au^- to 12 keV Au_2^- and 18 keV Au_3^- projectiles observed in Ref. 58, respectively, we find that for cluster sizes below $n=4$ the predictions from the simulation coincide almost quantitatively with the experimental data, whereas for larger clusters we observe even much larger enhancements than measured. In view of the fact that (i) the experimental data have been taken at a different kinetic impact energy per atom and (ii) secondary ions, i.e., those sputtered particles that leave the surface in an ionic charge state, are detected in the experiment, we consider this agreement satisfactory. It is known that the ionization probability of a sputtered particle may sensitively depend on details like the electronic structure of the escaping particle and the surface, and therefore secondary ions cannot generally be regarded as representative for sputtered fluxes. Moreover, it has been demonstrated that the probability of sputtered clusters to leave the surface as an ion generally depends on the cluster size.[65] In order to disentangle the effects of formation and ionization of sputtered clusters and, hence, generate experimental data which is better comparable with the simulations, it is therefore necessary to measure the mass distribution of sputtered *neutral* atoms and clusters as a function of the nuclearity of the projectile. Investigations of this type are currently underway in our laboratory.

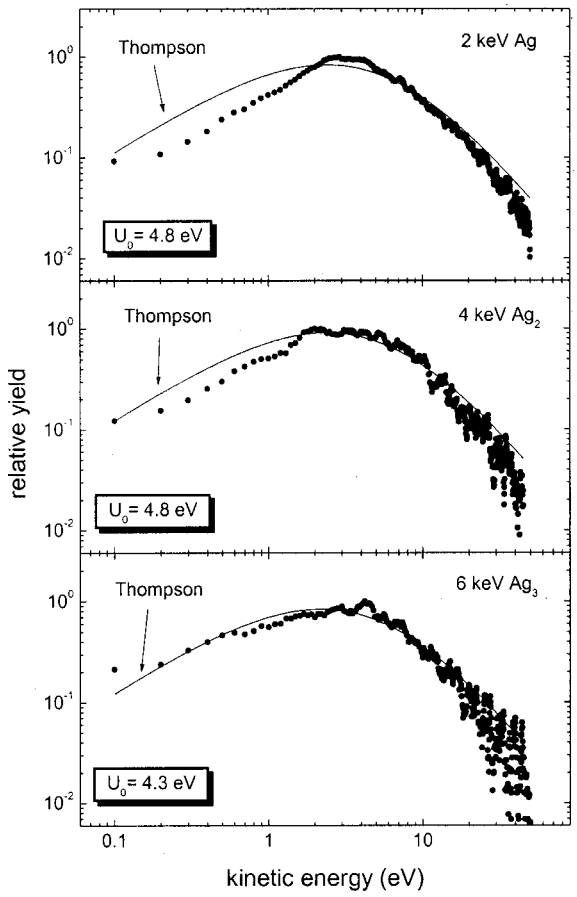

FIG. 10. Kinetic energy distribution of atoms sputtered from an Ag(111) surface under bombardment with monatomic, diatomic, and triatomic projectiles of 2 keV/atom. The solid line represents a fit of Eq. (8) to the data.

C. Kinetic energy distributions

When polyatomic projectiles are used to initiate a sputtering process, an interesting question arises as to which extent the nonlinear superposition of collision cascades leads to the development of collisional (sometimes incorrectly called ''thermal'') spikes. In a linear collision cascade, the density of moving particles is per definition low and, hence, every collision can be assumed to occur between a moving atom and an atom at rest. In a spike, on the other hand, the density of moving particles is high, and therefore many collisions between moving atoms occur. As a consequence, the characteristics of sputtered particles may change. In this context, the kinetic energy (or emission velocity) distribution of the sputtered particles has been suggested as a key quantity to distinguish spike contributions from linear collision processes. In particular, it is generally assumed that spike contributions manifest as additional low energy contributions in the energy spectrum of sputtered atoms.[66] In order to investigate this point, Fig. 10 shows the kinetic energy distribution of sputtered monomers which has been evaluated for monatomic, diatomic, and triatomic projectiles of the same impact velocity (corresponding to 2 keV/atom). For comparison, the prevailing formula predicted by linear cascade theory,[67]

$$f(E) \propto \frac{E}{(E+U_0)^3} \tag{8}$$

has been fitted to the data using the surface binding energy U_0 and the proportionality constant as fitting parameters. It is seen that the simulated distributions can be fairly well described by Eq. (8). Moreover, in the regime of small energies, where a low energy spike contribution should in principle manifest, the simulated distribution appears to be even *over*estimated by Eq. (8). The surface binding energy values resulting from the fit which are depicted in Fig. 10 are significantly larger than the sublimation energy of silver (3.0 eV). This finding is not unusual when comparing MD simulated data with the linear cascade theory prediction of Eq. (8).[44,68] Comparing the three distributions displayed in Fig. 10, no significant influence of the projectile nuclearity can be deduced except a slight apparent reduction of U_0 with increasing projectile size accompanied by a small relative enhancement in the low energy regime below 1 eV. The magnitude of the latter effect is less than a factor of 2 and therefore much less pronounced than similar effects observed

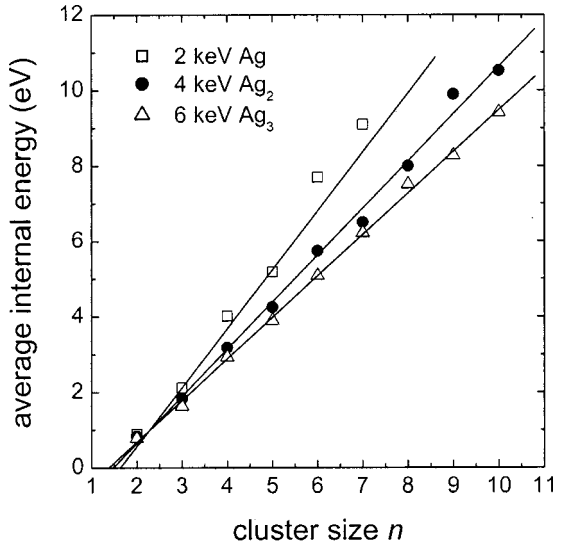

FIG. 11. Average internal energy of nascent clusters sputtered from an Ag(111) surface under bombardment with monatomic, diatomic, and triatomic projectiles of 2 keV/atom.

in Ref. 18. In conclusion, the kinetic energy distributions of sputtered atoms seem to indicate that in the case studied here the contribution of spike effects is small.

D. Internal energy distributions

As already stated in Sec. II, nascent clusters are identified among the cloud of sputtered particles immediately after the full MD simulation is terminated. Typically, this occurs at times of picoseconds after the projectile impact, when the sputtered clusters reside at distances of nanometers above the surface. At this point, we can determine the total internal energy of the cluster from the positions and velocities of the constituent atoms as described in Sec. II. Figure 11 shows the resulting average internal energy of sputtered clusters generated under monatomic, diatomic, and triatomic projectile bombardment. Since the dissociation thresholds of all clusters (as determined by the MD/MC-CEM potential) fall between 1.6 and 2.5 eV,[41] it is apparent that most of the nascent clusters are unstable and will hence undergo unimolecular fragmentation while moving farther away from the surface. It is interesting to note that in all three cases the average internal energy exhibits a linear dependence on the cluster size, a behavior which has been observed earlier for rare gas projectiles as well.[41] The slope, however, changes upon the transition from monatomic to polyatomic projectiles, thus indicating that nascent clusters produced by polyatomic projectile impacts are ''colder'' than those produced by monatomic projectiles. This finding is the more interesting in view of the fact that our previous studies employing exclusively monatomic projectiles revealed *no* influence of the projectile species (Ar or Xe) or kinetic energy (500 eV–5 keV) on the cluster size dependence of average internal energies. Moreover, the dependence observed here for monatomic projectiles is almost exactly identical with that determined for rare gas projectiles.[41] As a consequence, we conclude that the use of polyatomic projectiles generates a distinct difference with respect to the internal energy distribution of sputtered clusters which cannot be induced by monatomic projectiles. It is clear that such differences will significantly influence the unimolecular fragmentation chains undergone by such clusters on their path away from the surface and therefore translate to different fragment distributions which are then detected as final clusters. The data displayed in Fig. 11 therefore represent a key finding which indicates that the use of polyatomic projectiles with varying nuclearity may constitute a way to influence (and ultimately reduce) the fragmentation of sputtered molecules and clusters. It is evident that such a possibility will be of great importance for surface analytical techniques like Secondary Ion or Neutral Mass Spectrometry that are based on the mass spectrometric detection of sputtered molecules.

E. Lateral emission distribution

In order to gain more insight into the processes leading to particle ejection from the bombarded surface, it is of interest to investigate the spatial distribution of lattice sites around the projectile impact point from which the sputtered atoms originate. In particular, we are interested if this distribution changes with the nuclearity of the projectile. For monatomic and diatomic projectiles, respectively, more than 90% of the sputtered atoms stem from the uppermost atomic layer of the solid. For triatomic projectiles, this value is reduced to 81%, but still the large majority of sputtered atoms originates from the very surface. We therefore determine the sputtering probability of surface atoms as a function of their original lateral distance from the projectile impact point. In order to evaluate this distribution, the surface area of the model crystal is subdivided into 18 circular ring elements of a width corresponding to the nearest neighbor distance in the (111) plane which are centered around the impact point. For every calculated trajectory (i.e., projectile impact), the number of surface atoms ejected from each ring element is evalu-

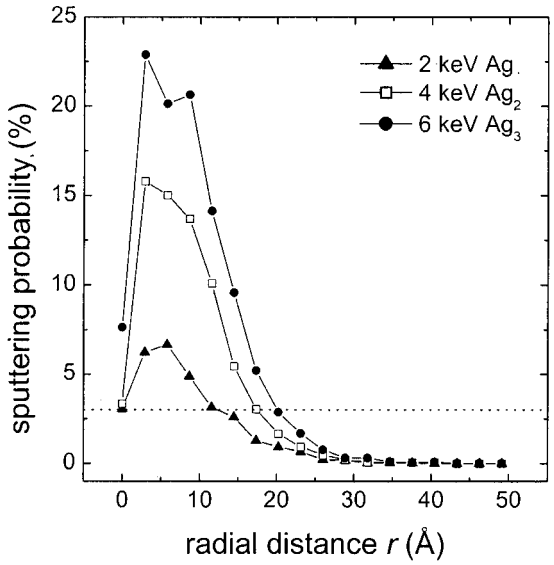

FIG. 12. Radial sputtering probability of surface atoms (i.e., atoms of the uppermost atomic layer) vs lateral distance of their original lattice location from the impact point. The three displayed curves correspond to bombardment with monatomic, diatomic, and triatomic projectiles impinging with the same velocity corresponding to an impact energy of 2 keV/atom.

TABLE I. Average sputtering yield, maximum value of the radial sputtering probability distribution, and effective surface area from which sputtered atoms are emitted vs projectile nuclearity at a bombarding energy of 2 keV/atom. For further explanation of the displayed quantities, see text.

Projectile nuclearity	Average sputtering yield	Maximum sputtering probability	Effective emission area
1	7	7%	450 Å^2
2	17	15%	1020 Å^2
3	31	22%	1390 Å^2

ated and normalized to the total number of lattice sites which fall within this element. In this procedure, only atoms from the uppermost atomic layer are counted regardless of their bonding state after ejection (sputtered monomers or part of an emitted cluster). The individual emission probabilities of each ring element are then averaged over all calculated trajectories of a simulation. Figure 12 shows the resulting radial distributions of the sputtering probability as a function of the distance from the impact point for monatomic, diatomic, and triatomic projectiles of the same impact velocity (corresponding to a kinetic energy of 2 keV per atom). It is seen that all three distributions start with a very low emission probability close to the impact point and peak at a radial distance of about 5 Å (corresponding to about two nearest neighbor distances). This behavior is very similar to that determined in Ref. 30 for polyatomic cluster bombardment of surfaces covered with organic molecules. As demonstrated therein, it reflects the fact that close to the impact point, where the energy density deposited by the projectile is high, most of the momentum is pointed towards the volume of the solid and therefore cannot induce sputtering action. At large distances, on the other hand, the emission probability naturally vanishes since the energy density deposited in the collision cascade becomes too low to induce sputtering. Interestingly, the three distributions of Fig. 12 look practically identical when normalized to their respective maxima. This means that the absolute values of the emission probabilities scale with the average sputtering yields when changing from one projectile to another, but otherwise the radial distribution remains practically unchanged. Using an arbitrary criterion of, for instance, a minimum emission probability of 3%, we can estimate an effective emission diameter of the collision cascade to be roughly 3 nm. Table I shows the resulting surface area from which sputtered particles originate together with the maximum sputtering probability and the average sputtering yield. It is seen that the emission area roughly scales with the maximum emission probability, whereas both quantities do not fully scale with the sputtering yield. This must be due to the fact that the fraction of second layer particles increases with increasing nuclearity of the projectile.

IV. CONCLUSION

Molecular dynamics have been employed to model the self sputtering phenomena occurring at a single crystal silver surface under bombardment with monatomic, diatomic and triatomic silver projectiles. For polyatomic projectiles, we observe a nonlinear enhancement of the sputtering yield per projectile atom with respect to monatomic projectiles of the same impact velocity. At first sight, the relatively small magnitude of this enhancement (19% for di- and 49% for triatomic projectiles) appears to be surprising in view of the large effects disclosed in Refs. 1, 6, 69, where enhancement factors up to 2.8 and 10.4 were measured for the transition from mono- to diatomic and from di- to triatomic projectiles of various elements bombarding silver, gold, and platinum surfaces, respectively. One must, however, keep in mind that the data published in these references have been obtained in a largely different range of impact energies (several 10 keV or even several 100 keV per atom) than employed here. Since the enhancement factors were in all cases found to decrease with decreasing impact energy per atom, it would be of great interest to compare our results with low energy experimental data which are unfortunately still lacking.

The simulations reveal that the abundance of both nascent and final clusters within the sputtered flux is enhanced when polyatomic instead of monatomic projectiles of the same impact velocity are used. Our data suggest that the effect is the more pronounced the larger the sputtered cluster. The magnitude of the enhancement appears to be larger upon switching from atomic to diatomic projectiles than upon switching from diatomic to triatomic projectiles. This finding is the more interesting, as we find a pronounced nonlinear enhancement of the total sputtering yield when using triatomic instead of diatomic projectiles. The power law exponent characterizing the size distribution of nascent clusters increases with increasing sputtering yield, but this increase seems to saturate towards high yields. It is shown that the saturation can be understood in terms of the statistics of the sputtering process. Comparing our simulations to available experimental data, we find that the magnitude of the enhancement observed in the simulations is in almost quantitative agreement with similar experimental data reported for secondary ion mass spectra of refractory metal surfaces. This indicates that at least part of the enhancement of secondary cluster ions and complex ionic species which has frequently been observed experimentally must be due to enhanced formation of the clusters in the course of the sputtering event.

From the radial distribution of the sputtering probability around the projectile impact point, we find that the enhancement in sputtering yield is accompanied by an increase of the effective emission area at the surface. The sputtering probability of surface atoms is increased with increasing projectile nuclearity, but otherwise the distribution seems to remain unchanged. Moreover, the kinetic energy distributions of sputtered atoms determined for different projectiles do not show distinct differences. According to the prevailing view, these observations would indicate that—for the impact energy range explored here—the nonlinear enhancement of sputtering yields and cluster abundances is not accompanied by a prominent collisional spike character of the collision cascade. We do, on the other hand, find characteristic differences of the internal energy distributions of sputtered nascent clusters which indicate that clusters produced under polyatomic projectile impacts are colder than those produced by monatomic projectiles. This result is the more interesting

since our previous simulations revealed that this distribution cannot be influenced by either the nature or the kinetic energy of the projectile as long as monatomic projectiles are used. It is therefore evident that the nature of the collision cascade leading to sputter ejection of particles must change upon the transition from monatomic to polyatomic projectiles. We therefore suggest that the internal energy distribution of sputtered clusters may be even more indicative of collisional spike contributions than the kinetic energy distribution of sputtered atoms. A visual inspection of some of the simulated trajectories reveals that at least those events producing high yields and, hence, large sputtered clusters under triatomic projectile bombardment clearly show the long duration and high density of moving atoms which is—by definition—characteristic for a spike.

ACKNOWLEDGMENTS

The authors would like to thank A. E. DePristo for making the MD/MC-CEM potential available to us. B.J.G. acknowledges financial support from the Chemistry Division of the National Science Foundation.

[1] H. H. Andersen and H. L. Bay, J. Appl. Phys. **45**, 953 (1974).
[2] H. H. Andersen and H. L. Bay, J. Appl. Phys. **46**, 2416 (1975).
[3] H. H. Andersen, Mat. Fys. Medd. K. Dan. Vidensk. Selsk. **43**, 127 (1993).
[4] D. A. Thompson and S. S. Johar, Appl. Phys. Lett. **34**, 342 (1979).
[5] D. A. Thompson and S. S. Johar, Nucl. Instrum. Methods **170**, 281 (1980).
[6] H. H. Andersen, A. Brunelle, S. Della-Negra, J. Depauw, D. Jacquet, Y. Le Beyec, J. Chaumont, and H. Bernas, Phys. Rev. Lett. **80**, 5433 (1998).
[7] Y. Le Beyec, Int. J. Mass Spectrom. Ion Processes **174**, 101 (1998).
[8] S. F. Belykh, U. K. Rasulev, A. V. Samartsev, and I. V. Veryovkin, Nucl. Instrum. Methods Phys. Res. B **136-138**, 773 (1998).
[9] K. Baudin, A. Brunelle, S. Della-Negra, D. Jacquet, P. Håkansson, Y. Le Beyec, M. Pautrat, R. R. Pinho, and C. Schoppmann, Nucl. Instrum. Methods Phys. Res. B **112**, 59 (1996).
[10] A. Brunelle, S. Della-Negra, J. Depauw, D. Jacquet, Y. Le Beyec, M. Pautrat, and C. Schoppmann, Nucl. Instrum. Methods Phys. Res. B **125**, 207 (1997).
[11] K. Boussofiane-Baudin, A. Brunelle, P. Chaurand, S. Della-Negra, J. Depauw, P. Håkansson, and Y. Le Beyec, Nucl. Instrum. Methods Phys. Res. B **88**, 61 (1994).
[12] T. Muramoto and Y. Yamamura, in *Similarities and Differences between Atomic Nuclei and Clusters. Toward a Unified Development of Cluster Science*, edited by Y. Abe, I. Arai, S.M. Lee, and K. Yabana (AIP Conference Proc. 41G, 1998), p. 487.
[13] Y. Yamamura and T. Muramoto, Radiat. Eff. **130-131**, 225 (1994).
[14] Y. Yamamura and T. Muramoto, Phys. Rev. Lett. **69**, 1463 (1992).
[15] Y. Yamamura, Nucl. Instrum. Methods Phys. Res. B **45**, 707 (1990).
[16] Y. Yamamura, Nucl. Instrum. Methods Phys. Res. B **33**, 493 (1988).
[17] M. H. Shapiro and T. A. Tombrello, Surf. Sci. **453**, 143 (2000).
[18] M. H. Shapiro and T. A. Tombrello, Nucl. Instrum. Methods Phys. Res. B **152**, 221 (1999).
[19] A. M. Childs, M. H. Shapiro, and T. A. Tombrello, Nucl. Instrum. Methods Phys. Res. B **143**, 298 (1998).
[20] M. H. Shapiro, G. A. Tosheff, and T. A. Tombrello, Nucl. Instrum. Methods Phys. Res. B **88**, 81 (1994).
[21] M. H. Shapiro and T. A. Tombrello, Radiat. Eff. **130-131**, 235 (1994).
[22] M. H. Shapiro and T. A. Tombrello, Nucl. Instrum. Methods Phys. Res. B **58**, 161 (1991).
[23] M. H. Shapiro and T. A. Tombrello, Mod. Phys. Lett. B **5**, 341 (1991).
[24] M. H. Shapiro and T. A. Tombrello, Phys. Rev. Lett. **65**, 92 (1990).
[25] M. H. Shapiro and T. A. Tombrello, Nucl. Instrum. Methods Phys. Res. B **48**, 557 (1990).
[26] G. Betz and W. Husinsky, Nucl. Instrum. Methods Phys. Res. B **122**, 311 (1997).
[27] T. J. Colla, R. Aderjan, R. Kissel, and H. M. Urbassek, Phys. Rev. B **62**, 8487 (2000).
[28] R. Aderjan and H. M. Urbassek, Nucl. Instrum. Methods Phys. Res. B **164-165**, 697 (2000).
[29] T. J. Colla and H. M. Urbassek, Nucl. Instrum. Methods Phys. Res. B **164-165**, 687 (2000).
[30] D. W. Ward, T. C. Nguyen, and K. D. Krantzman, *Secondary Ion Mass Spectrometry (SIMS XII)*, edited by A. Benninghoven, P. Bertrand, H. N. Migeon, and H. W. Werner (Elsevier Science, New York, 2000), p. 183.
[31] R. Žaric, B. Pearson, K. D. Krantzman, and B. J. Garrison, *Secondary Ion Mass Spectrometry (SIMS XI)*, edited by G. Gillen, R. Lareau, J. Bennett, and F. Stevie (Wiley, New York, 1998), p. 601.
[32] R. Žaric, B. Pearson, K. D. Krantzman, and B. J. Garrison, Int. J. Mass Spectrom. Ion Processes **174**, 155 (1998).
[33] Z. Insepov and I. Yamada, Nucl. Instrum. Methods Phys. Res. B **112**, 16 (1996).
[34] Z. Insepov and I. Yamada, Nucl. Instrum. Methods Phys. Res. B **99**, 248 (1995).
[35] K. Johannessen, Nucl. Instrum. Methods Phys. Res. B **73**, 481 (1993).
[36] S. R. Coon, W. F. Calaway, and M. J. Pellin, Nucl. Instrum. Methods Phys. Res. B **90**, 518 (1994).
[37] Z. Ma, S. R. Coon, W. F. Calaway, M. J. Pellin, D. M. Gruen, and E. I. Nagy-Felsobuki, J. Vac. Sci. Technol. **A 12**, 2425 (1994).
[38] S. R. Coon, W. F. Calaway, M. J. Pellin, and J. M. White, Surf. Sci. **298**, 161 (1993).
[39] S. R. Coon, W. F. Calaway, J. W. Burnett, M. J. Pellin, D. M. Gruen, D. R. Spiegel, and J. M. White, Surf. Sci. **259**, 275 (1991).
[40] A. Wucher and M. Wahl, *Secondary Ion Mass Spectrometry (SIMS X)*, edited by A. Benninghoven, B. Hagenhoff, and H. W. Werner (Wiley, New York, 1997), p. 64.
[41] A. Wucher and B. J. Garrison, J. Chem. Phys. **105**, 5999 (1996).
[42] A. Wucher and M. Wahl, Nucl. Instrum. Methods Phys. Res. B **115**, 581 (1996).
[43] D. E. Harrison, Jr., P. W. Kelly, B. J. Garrison, and N. Winograd, Surf. Sci. **76**, 311 (1978).
[44] B. J. Garrison, N. Winograd, D. M. Deaven, C. T. Riemann, D. Y. Lo, T. A. Tombrello, D. E. Harrison, Jr., and M. H. Shapiro, Phys. Rev. B **37**, 7197 (1988).
[45] C. L. Kelchner, D. M. Halstead, L. S. Perkins, N. M. Wallace, and A. E. DePristo, Surf. Sci. **310**, 425 (1994).
[46] T. J. Raeker and A. E. DePristo, Int. Rev. Phys. Chem. **10**, 1 (1991).
[47] A. Wucher and B. J. Garrison, Phys. Rev. B **46**, 4855 (1992).
[48] O. Almén and G. Bruce, Nucl. Instrum. Methods **11**, 279 (1961).
[49] M. Wahl and A. Wucher, Nucl. Instrum. Methods Phys. Res. B **94**, 36 (1994).
[50] C. E. Young, D. R. Spiegel, M. J. Pellin, W. F. Calaway, S. R. Coon, J. W. Burnett, D. M. Gruen, A. M. Davis, and R. N. Clayton, *Resonance Ionization Spectroscopy 1990*, edited by J. E. Parks and N. Omenetto (Institute of Physics, Bristol, 1991), p. 435.
[51] C. Staudt, R. Heinrich, and A. Wucher, Nucl. Instrum. Methods Phys. Res. B **164-165**, 677 (2000).
[52] T. J. Colla, H. M. Urbassek, A. Wucher, C. Staudt, R. Heinrich, B. J. Garrison, C. Dandachi, and G. Betz, Nucl. Instrum. Methods Phys. Res. B **143**, 284 (1998).
[53] A. Wucher, Nucl. Instrum. Methods Phys. Res. B **83**, 79 (1993).
[54] A. Brunelle, S. Della-Negra, J. Depauw, D. Jacquet, Y. Le Beyec, M. Pautrat, K. Baudin, and H. H. Andersen, Phys. Rev. A **63**, 022902 (2001).
[55] K. Baudin, A. Brunelle, S. Della-Negra, J. Depauw, and Y. Le Beyec, *Secondary Ion Mass Spectrometry (SIMS XI)*, edited by G. Gillen, R. Lareau, J. Bennett, and F. Stevie (Wiley, New York, 1998), p. 597.
[56] K. Boussofiane-Baudin, G. Bolbach, A. Brunelle, S. Della-Negra, P. Håkansson, and Y. Le Beyec, Nucl. Instrum. Methods Phys. Res. B **88**, 160 (1994).
[57] M. Benguerba, A. Brunelle, S. Della-Negra, J. Depauw, H. Joret, Y. Le Beyec, M. G. Blain, E. A. Schweikert, G. Ben Assayag, and P. Sudraud, Nucl. Instrum. Methods Phys. Res. B **62**, 8 (1991).
[58] S. F. Belykh, B. Habets, U. Kh. Rasulev, A. V. Samartsev, L. V. Stroev, and I. V. Veryovkin, Nucl. Instrum. Methods Phys. Res. B **164-165**, 809 (2000).
[59] S. F. Belykh, B. Habets, U. Kh. Rasulev, A. V. Samartsev, and L. V. Stroev, *Secondary Ion Mass Spectrometry (SIMS XII)*, edited by A. Benninghoven, P. Bertrand, H. N. Migeon, and H. W. Werner (Elsevier, New York, 2000), p. 275.
[60] S. F. Belykh, U. K. Rasulev, A. V. Samartsev, S. V. Verkhoturov, and I. V. Veryovkin, Mikrochim. Acta **15**, 379 (1998).
[61] S. F. Belykh, V. I. Matveev, U. Kh. Rasulev, A. V. Samartsev, and I. V.

Veryovkin, *Secondary Ion Mass Spectrometry (SIMS XI)*, edited by G. Gillen, R. Lareau, J. Bennett, and F. Stevie (Wiley, New York, 1998), p. 957.
[62] S. F. Belykh, I. S. Bitensky, D. Mullajanov, and U. K. Rasulev, Nucl. Instrum. Methods Phys. Res. B **129**, 451 (1997).
[63] M. G. Blain, S. Della-Negra, H. Joret, Y. Le Beyec, and E. A. Schweikert, Phys. Rev. Lett. **63**, 1625 (1989).
[64] M. G. Blain, S. Della-Negra, H. Joret, Y. Le Beyec, and E. A. Schweikert, J. Phys. (Paris) **50**, C2-147 (1989).
[65] R. Heinrich, C. Staudt, M. Wahl, and A. Wucher, *Secondary Ion Mass Spectrometry (SIMS XII)*, edited by A. Benninghoven, P. Bertrand, H. N. Migeon, and H. W. Werner (Elsevier Science, New York, 2000), p. 111.
[66] M. Szymonski and A. Poradzisz, Appl. Phys. A: Solids Surf. **28**, 175 (1982).
[67] M. W. Thompson, Philos. Mag. **18**, 377 (1968).
[68] B. J. Garrison, Nucl. Instrum. Methods Phys. Res. B **40-41**, 313 (1988).
[69] S. S. Johar and D. A. Thompson, Surf. Sci. **90**, 319 (1979).